SKYRME-HARTREE-FOCK DESCRIPTION OF THE DIPOLE STRENGTH IN NEUTRON-RICH TIN ISOTOPES

J. KVASIL[1], V. O. NESTERENKO[2], W. KLEINIG[2,3], D. BOŽÍK[1], and P.-G. REINHARD[4]

[1]*Institute of Particle and Nuclear Physics,*

Charles University, CZ-18000 Praha, Czech Republic

kvasil@ipnp.troja.mff.cuni.cz; bozik@ipnp.troja.mff.cuni.cz

[2]*BLTP, Joint Institute for Nuclear Research,*

141980, Dubna, Moscow region, Russia

nester@theor.jinr.ru; kleinig@theor.jinr.ru

[3]*Technische Universität Dresden, Inst. für Analysis, D-01062, Dresden, Germany. and*

[4]*Institut für Theoretische Physik II, Universität Erlangen, D-91058, Erlangen, Germany;*

mpt218@theorie2.physik.uni-erlangen.de

(Dated: today)

Abstract

Low-energy E1 strength in neutron-rich $^{132-164}$Sn isotopes is analyzed in the framework of the Skyrme random phase approximation (RPA) with different Skyrme forces. A double folding procedure is applied to take into account the energy-dependent width effects beyond RPA. All the considered Skyrme forces indicate a soft prolate deformation in the open shell isotopes $^{142-164}$Sn. The integrated E1 strength in the energy region of the pygmy resonance grows with the neutron number. The influence of deformation on the integrated strength near the particle emission thresholds (which is of a keen astrophysical interest) is strictly suppressed by the mutual compensation effect for the branches of the giant dipole resonance. The results obtained are in a good agreement with the previous findings of the relativistic mean field model.

1

I. INTRODUCTION

Exotic nuclear collective excitations, like the dipole pygmy mode (PM), represent a subject of intense investigations during last decades, see the recent review [1]. The analysis of these excitations provides a deeper insight into nuclear dynamics. Besides, the PM affects the E1 strength near the particle emission thresholds, which is of a key interest for astrophysical applications [1, 2]. The PM is viewed as a vibration of the neutron skin against the isospin-saturated proton-neutron core [1]. In this connection, the evolution of PM with rising the neutron number and approaching the neutron drip line attracts a large attention.

The available experimental data show the growth of PM strength with neutron excess in medium-heavy [3–5] and light [6, 7] *stable* nuclei. This trend was confirmed by relativistic and non-relativistic (Skyrme) mean-field calculations [1]. Meanwhile, the experimental effort focuses on drip-line regions and thus a theoretical analysis of the PM behaviour in unstable nuclei is required. Such study was recently performed for neutron-rich $^{132-166}$Sn isotopes within the relativistic mean-field model (RMF) [8]. A growth of PM strength with the neutron number was confirmed and a region of deformed isotopes $^{142-162}$Sn with more spread of the strength was predicted.

The aim of present paper is to investigate the deformation and neutron-excess effects in the $^{132-166}$Sn chain within the Skyrme mean-field approach. The separable random-phase-approximation (SRPA) model [9, 10] is used. SRPA is fully self-consistent as both the static mean field and residual interaction are derived from the same Skyrme functional. The model covers both spherical and axially-deformed nuclei. It was already applied to describe electric [9–12] and magnetic [13, 14] giant resonances as well as the E1 strength near the particle thresholds [15]. In the present paper, the SRPA formalism is supplemented by the double folding procedure which allows to compute strength functions with an energy-dependent width. The SRPA analysis below is done with the representative set of Skyrme forces, SkT6 [16], SkM* [17], SLy6 [18], and SkI3 [19], covering a broad interval of Skyrme parameters and nuclear matter characteristics.

II. SRPA APPROACH

SRPA is derived from the Skyrme energy functional [20]

$$E(\rho, \tau, \mathbf{s}, \mathbf{J}, \mathbf{T}, \chi) = \int \mathcal{H}(\mathbf{r}) d\mathbf{r} \qquad (1)$$

involving time-even (nucleon ρ_q, kinetic-energy τ_q, spin-orbit $\mathbf{J}_q$) and time-odd (current $\mathbf{j}_q$, spin $\mathbf{s}_q$, vector kinetic-energy $\mathbf{T}_q$) densities, as well as the pairing density χ_q. The index q stands for

neutrons $(q = n)$ and protons $(q = p)$.

The energy density $\mathcal{H}(\mathbf{r})$ consists of the kinetic-energy $\mathcal{H}_{\text{kin}}(\mathbf{r})$, Skyrme $\mathcal{H}_{Sk}(\mathbf{r})$, pairing $\mathcal{H}_{\text{pair}}(\mathbf{r})$, and Coulomb $\mathcal{H}_{\text{Coul}}(\mathbf{r})$ contributions

$$\mathcal{H}(\mathbf{r}) = \mathcal{H}_{\text{kin}}(\mathbf{r}) + \mathcal{H}_{Sk}(\mathbf{r}) + \mathcal{H}_{\text{pair}}(\mathbf{r}) + \mathcal{H}_{\text{Coul}}(\mathbf{r}) \tag{2}$$

where

$$\mathcal{H}_{\text{kin}}(\mathbf{r}) = \frac{\hbar^2}{2m}\tau , \tag{3}$$

$$\begin{aligned}
\mathcal{H}_{\text{Sk}}(\mathbf{r}) = & \frac{b_0}{2}\rho^2 - \frac{b_0'}{2}\sum_q \rho_q^2 + \frac{b_3}{3}\rho^{\alpha+2} - \frac{b_3'}{3}\rho^\alpha \sum_q \rho_q^2 \\
& + b_1(\rho\tau - \mathbf{j}^2) - b_1'\sum_q(\rho_q\tau_q - \mathbf{j}_q^2) - \frac{b_2}{2}\rho\Delta\rho + \frac{b_2'}{2}\sum_q \rho_q\Delta\rho_q \\
& - b_4(\rho\nabla\mathbf{J} + (\nabla\times\mathbf{j})\mathbf{s}) - b_4'\sum_q(\rho_q\nabla\mathbf{J}_q + (\nabla\times\mathbf{j}_q)\mathbf{s}_q) \\
& + \frac{\tilde{b}_0}{2}\mathbf{s}^2 - \frac{\tilde{b}_0'}{2}\sum_q \mathbf{s}_q^2 + \frac{\tilde{b}_3}{3}\rho^\alpha \mathbf{s}^2 - \frac{\tilde{b}_3'}{3}\rho^\alpha \sum_q \mathbf{s}_q^2 - \frac{\tilde{b}_2}{2}\mathbf{s}\cdot\Delta\mathbf{s} + \frac{\tilde{b}_2'}{2}\sum_q \mathbf{s}_q\cdot\Delta\mathbf{s}_q \\
& + \tilde{b}_1(\mathbf{s}\cdot\mathbf{T} - \mathbf{J}^2) + \tilde{b}_1'\sum_q(\mathbf{s}_q\cdot\mathbf{T}_q - \mathbf{J}_q^2) ,
\end{aligned} \tag{4}$$

$$\mathcal{H}_{\text{pair}}(\mathbf{r}) = \frac{1}{4}\sum_q \chi_q^2 V_q \left[1 - \left(\frac{\rho}{\rho_0}\right)^\gamma\right] , \tag{5}$$

$$\mathcal{H}_{\text{Coul}}(\mathbf{r}) = \frac{e^2}{2}\int d\mathbf{r}' \rho_p(\mathbf{r})\frac{1}{|\mathbf{r} - \mathbf{r}'|}\rho_p(\mathbf{r}') - \frac{3}{4}e^2\left(\frac{3}{\pi}\right)^{1/3}[\rho_p(\mathbf{r})]^{3/4} \tag{6}$$

where the densities without index, like $\rho = \rho_p + \rho_n$, are total. The explicit expressions for the densities can be found elsewhere [10]. In the part (5), V_q is the pairing strength and ρ_0 is the equilibrium nuclear matter density. The pairing is treated at the BCS level. The Coulomb contribution includes direct and exchange terms. In the part (4), the Skyrme terms with the tilded parameters $\tilde{b}_i$ and $\tilde{b}_i'$ are relevant only for magnetic excitations and so are omitted in the present study.

The self-consistent derivation [9, 10] gives from (1)-(6) the SRPA Hamiltonian

$$\hat{H} = \hat{h}_{\text{HFB}} + \hat{V}_{\text{res}} \tag{7}$$

where $\hat{h}_{\text{HFB}}$ is the HFB mean field

$$\hat{h}_{\text{HFB}} = \int d\mathbf{r}\sum_{\alpha_+}\left[\frac{\partial E}{\partial J_{\alpha_+}(\mathbf{r})}\right]\hat{J}_{\alpha_+}(\mathbf{r}) \tag{8}$$

and $\hat{V}_{\text{res}}$ is the separable residual interaction

$$\hat{V}_{res} = \frac{1}{2}\sum_{k,k'=1}^{K}\left[\kappa_{kk'}\hat{X}_k\hat{X}_{k'} + \eta_{kk'}\hat{Y}_k\hat{Y}_{k'}\right] \tag{9}$$

with one-body operators

$$\hat{X}_k = i \int d\mathbf{r} \int d\mathbf{r}' \sum_{\alpha_+,\alpha'_+} \left[\frac{\partial^2 E}{\partial J_{\alpha_+}(\mathbf{r}')\partial J_{\alpha_+}(\mathbf{r})} \right] \langle | \left[\hat{P}_k, \hat{J}_{\alpha_+}(\mathbf{r}) \right] | \rangle \hat{J}_{\alpha'_+}(\mathbf{r}') ,$$

$$\hat{Y}_k = i \int d\mathbf{r} \int d\mathbf{r}' \sum_{\alpha_-,\alpha'_-} \left[\frac{\partial^2 E}{\partial J_{\alpha_-}(\mathbf{r}')\partial J_{\alpha_-}(\mathbf{r})} \right] \langle | \left[\hat{Q}_k, \hat{J}_{\alpha_-}(\mathbf{r}) \right] | \rangle \hat{J}_{\alpha'_-}(\mathbf{r}') \tag{10}$$

and inverse strength matrices

$$\kappa_{kk'}^{-1} = -i\langle[\hat{P}_k, \hat{X}_{k'}]\rangle , \quad \eta_{kk'}^{-1} = -i\langle[\hat{Q}_k, \hat{Y}_{k'}]\rangle . \tag{11}$$

Here $\alpha_+ = \rho, \tau, \mathbf{J}, \chi$ and $\alpha_- = \mathbf{j}, \mathbf{s}, \mathbf{T}$ enumerate time-even J_{α_+} and time-odd J_{α_-} densities; $\hat{J}_{\alpha_\pm}$ are the density operators; $\hat{Q}_k$ and $\hat{P}_k = i[\hat{H}, \hat{Q}_k]$ are time-even and time-odd hermitian input operators chosen following the procedure [10, 12]. The operators of the residual interaction $\hat{X}_k$ and $\hat{Y}_k$ are time-even and time-odd, respectively. The single-particle Hamiltonian $\hat{h}_{\text{HFB}}$ is determined by the first functional derivatives of the initial functional (1) while operators $\hat{X}_k$ and $\hat{Y}_k$ are driven by the second functional derivatives of the same functional. Hence the model is fully self-consistent. The number K of separable terms is determined by the number of the input operators $\hat{Q}_k$. Usually we have $K = 3 - 5$. Hence a low rank of the RPA matrix and minor computational effort even for heavy deformed nuclei.

When studying giant resonances, one is usually interested in the strength function. For electric dipole excitations, the strength function reads

$$S_{E1}(E) = \sum_{\mu} S_{E1\mu}(E), \quad S_{E1\mu}(E) = \sum_{\nu} E_\nu |\langle \nu | \hat{f}_{E1\mu} | \rangle|^2 \zeta_\Delta(E - E_\nu) \tag{12}$$

where $\hat{f}_{E1\mu} = \sum_i e_i^{\text{eff}} e r Y_{1\mu}$ is operator of $E1\mu$-transition with the effective charges $e_p^{\text{eff}} = N/A$ and $e_n^{\text{eff}} = -Z/A$ and

$$\zeta_\Delta(E - E_\nu) = \frac{1}{2\pi} \frac{\Delta}{(E - E_\nu)^2 + \left(\frac{\Delta}{2}\right)^2} \tag{13}$$

is the Lorentz weight with the averaging parameter Δ to simulate the smoothing effects beyond SRPA (escape widths and coupling to complex configurations). The strength function is composed by computing the detailed RPA spectrum E_ν and reduced transition probabilities $B(E1, \nu) = |\langle \nu | \hat{f}_{E1\mu} | \rangle|^2$. However it is more convenient to compute the strength function directly by using the linear response techniques [9, 10] for which the factorization (9) additionally simplifies the calculation. We thus use this direct technique.

The actual smoothing effects depend on the excitation energy E. The escape widths appear above the particle emission thresholds and grow with energy due to widening of the emission phase

space. The coupling with complex configurations (collisional width) also increases with energy. To take into account these trends, one should use in (12)-(13) an energy-dependent averaging parameter $\Delta(E)$. This can be done by implementation of the double folding scheme which allows to use the strength function formalism (with fixed width) for the RPA solutions. At the first step, we calculate the strength function (12) with a small but fixed value of Δ. This gives the strength distribution $S_{E1\mu}(E')$ very close to the actual RPA one but for the equidistant energy grid. At the next step, this strength is additionally folded by using the energy dependent averaging $\Delta(E)$:

$$S'_{E1}(E) = \int dE' \, S_{E1}(E')\xi_{\Delta(E')}(E - E') \,. \tag{14}$$

In the present study we use the simple linear energy dependence

$$\Delta(E') = \begin{cases} \Delta_0 & \text{for } E' \leq E_{\text{th}} \\ \Delta_0 + a(E' - E_{\text{th}}) & \text{for } E' > E_{\text{th}} \end{cases} \tag{15}$$

where E_{th} is the energy of the first emission threshold and Δ_0 is a minimal width describing the coupling with complex configurations below the threshold. The rate a is chosen to give a proper reproduction of the form of the giant dipole resonance (GDR). In the present study, we use $\Delta_0 = 0.1$ MeV and $a = 1/6$.

The dipole photoabsorption cross section is related to the strength function (12) as $\sigma(E) \approx 0.402 S_{E1}(E)$ with $S_{E1}(E)$ being in $e^2\text{fm}^2$ and $\sigma(E)$ in fm^2.

III.   RESULTS AND DISCUSSION

The results are obtained for the representative set of Skyrme forces: SkT6 [16], SkM* [17], SLy6 [18], and SkI3 [19]. These forces have different nuclear matter characteristics and are widely used for the description of ground state properties and dynamics of atomic nuclei [20], including deformed ones. The calculations use a cylindrical coordinate-space grid with the mesh size 0.7 fm. The equilibrium quadrupole deformations are found by minimization of the total energy of the system.

In Fig.1 the calculated equilibrium quadrupole deformations β in Sn isotopes with $100 \leq A \leq 166$ are shown for the four different Skyrme forces. The broad mass region involves neutron-deficient, stable, and neutron-rich nuclei. The deformations are given for the total, neutron, and proton densities. The results are compared with the RMF findings [8]. It is seen that for $A \leq 140$ the isotopes keep the spherical shape, for exception of a narrow region $112 \leq A \leq 116$ where forces SkT6, SLy6, and SkI3 predict some oblate softness. It is remarkable that, despite the semi-magic
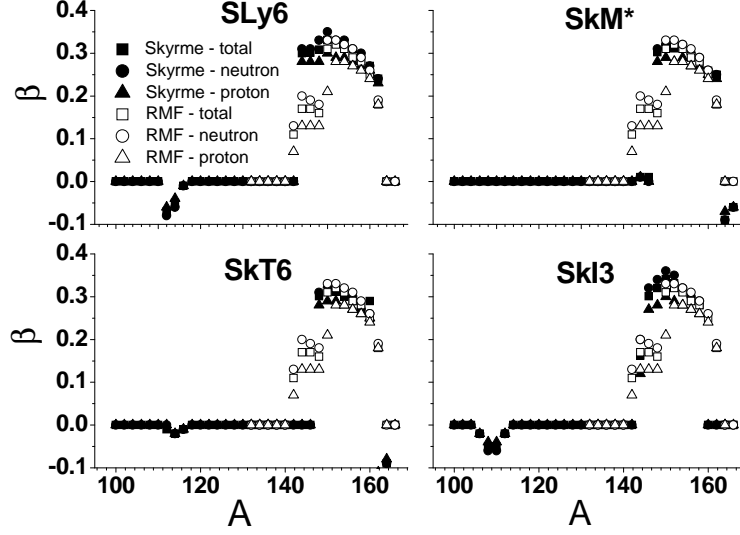
5

FIG. 1: Equilibrium total, neutron and proton quadrupole deformations in $^{100-166}$Sn, calculated with Skyrme forces SLy6, SkM*, SkT6, and SkI3 and compared to the RMF results [8].
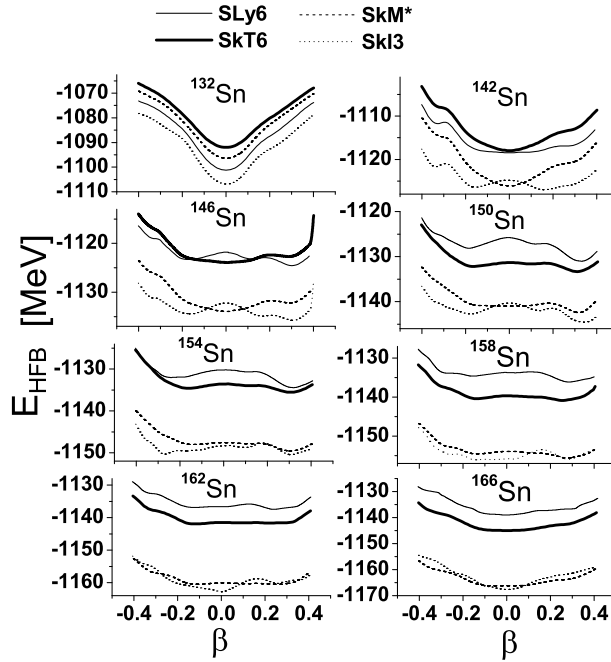

FIG. 2: Dependence of the HFB nuclear energy on the total quadrupole deformation β for SkT6, SLy6, SkM*, and SkI3 forces in selected neutron-rich Sn isotopes.

character of Sn isotopes (Z=50), they exhibit a significant prolate deformation in the neutron-rich region $142 \leq A \leq 162$, which is in accordance to RMF predictions [8]. Note that neutron deformation in this region is systematically larger than the proton ones, which may signify the
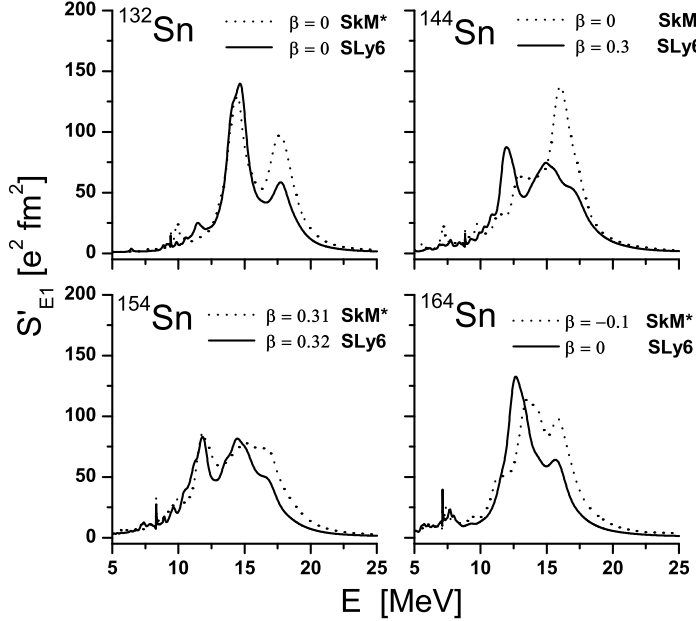
FIG. 3: The doubly folded E1 strength function for SkM* and SLy6 in selected Sn isotopes.

higher deformation of the excess neutrons. Perhaps, just the drive of the large neutron skin to the deformation causes the whole effect in these semi-magic nuclei which otherwise might be spherical as in the neutron-deficit region.

The further analysis shows that $^{142-162}$Sn isotopes should be rather considered as prolate-soft instead of prolate-deformed. Indeed, the total HFB energies E_{HFB} depicted in Fig. 2 demonstrate for $142 \leq A \leq 162$ very shallow deformation minima. Though the deformations and E_{HFB} values in the transition regions with A=142-146 and 158-162 noticeably vary with the force (in some cases, e. g. for SkI3 in ^{154}Sn, both prolate and oblate minima are predicted), the results for different forces are qualitatively similar. Altogether they point out to possible strong softness and anharmonicity in $^{142-162}$Sn.

In Fig. 3, the doubly folded strength function $S'_{E1}(E)$ is shown for the forces SkM* and SLy6 in the representative isotopes (spherical ^{132}Sn, transition ^{144}Sn, deformed ^{154}Sn, and spherical ^{164}Sn) covering the deformation region and its vicinities. The double folding is computed with the threshold energies (associated to the neutron single-particle Fermi levels) marked in Fig. 4. It gives a reasonable width $\Delta \sim 1$ MeV at the GDR peak. Due to larger averaging at higher energies, the double folding considerably suppress the artificial strong shoulder at the right GDR side, which often appears in Skyrme-RPA calculations both with [9, 11, 12] and without [21] the separable
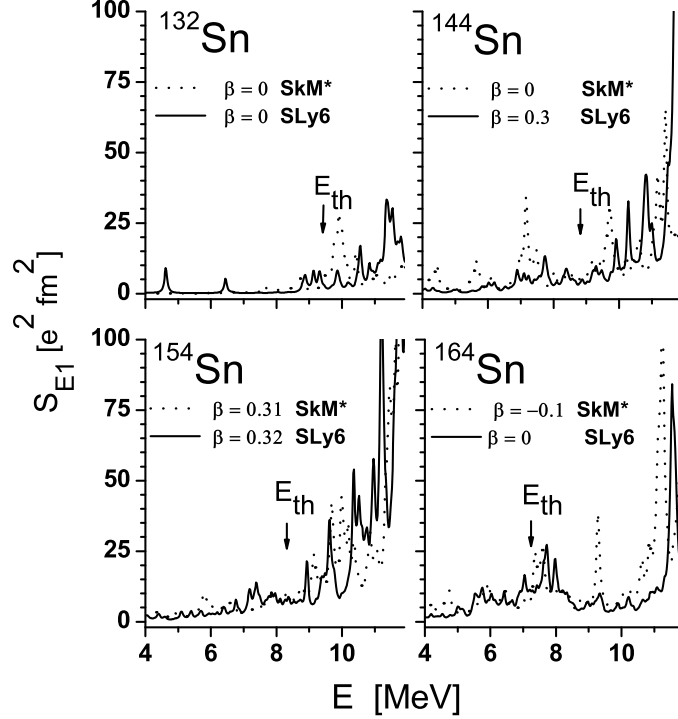
FIG. 4: The low-energy E1 strength function (with constant $\Delta = 0.1$ MeV) for SkM* and SLy6 in selected Sn isotopes. The estimated particle emission thresholds E_{th} are marked by arrows.

prescription. Fig. 3 shows that SkM* and SLy6 give similar shapes for spherical and deformed isotopes but rather different deformations in transition ^{144}Sn. Some fine structures are seen in the pygmy energy region 5-10 MeV. The E1 strength in this region grows with the neutron number.

The latter effect is better visible in Fig. 4 where the E1 strength function (12) is exhibited with a small constant averaging $\Delta = 0.1$ MeV in the low-energy pygmy region. It is seen that fine structure of the strength significantly depends on the force and it is more separated from the GDR in spherical isotopes than in deformed ones. Hence, in accordance to RMF results [8], spherical nuclei are indeed more suitable for observation of the pygmy mode. Note also that pygmy energy regions stay near the particle emission thresholds and so the pygmy resonance may affect the near-threshold E1 strength of the astrophysical interest [1, 2, 15].

In Fig. 5, the pygmy nature of the low-energy strength is illustrated for particular RPA states in spherical ^{132}Sn and ^{164}Sn. It is seen that in the nuclear surface at 6-8 fm the neutron transition density dominates thus manifesting the oscillation of the neutron excess against the proton-neutron core.
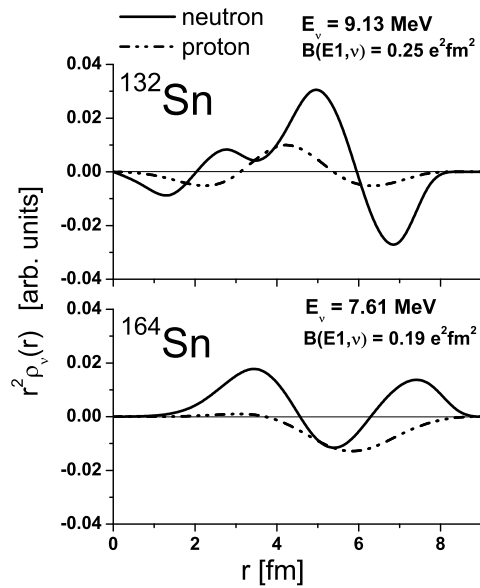
FIG. 5: Neutron and proton transition densities $\rho_\nu(r)$ in particular low-energy RPA ν-states with large $B(E1,\nu)$ values in spherical ^{132}Sn and ^{164}Sn. The force SLy6 is used.

Finally Fig. 6 shows the integrated E1 photoabsorption cross section

$$\Sigma(E) = \int_{4\mathrm{MeV}}^{E} \sigma(E')\mathrm{d}E' \tag{16}$$

in units of the Thomas-Reiche-Kuhn (TRK) sum rule $\sum_{TRK} = 60NZ/A$ mb MeV. The upper panel compares the ratios in spherical ^{132}Sn and deformed ^{154}Sn. At $E > 7$ MeV the isotope ^{154}Sn delivers more low-energy E1 strength. This may be caused by two factors in ^{154}Sn, the deformation and the larger mass number. The deformation down-shifts the left μ=0 GDR branch and the larger nuclear size down-shifts the GDR in general. While the latter factor is clear, the effect of deformation deserves more analysis [15, 22, 23]. It is inspected for ^{154}Sn in the lower panel of Fig. 6. The comparison of the photoabsorption cross sections for equilibrium deformation $\beta = 0.316$ and deliberately constrained spherical case $\beta = 0$ shows that the deformation results in a larger cumulative strength only at $E > 10$ MeV, i.e. in a close vicinity to the GDR. Instead, at the lower energies near thresholds (the region of the astrophysical interest) the deformation leads, in fact, to a weak depletion of the strength.

The weak deformation effect in the pygmy region can be explained by the destructive competition of $\mu = 0$ and $\mu = 1$ GDR contributions to the low-energy E1 strength [15]. As seen from Fig. 6, both these GDR branches affect the pygmy region and the $\mu = 0$ branch evidently dominates. However, at low energies far enough from the GDR ($E < 10$ MeV in our case), the influences of
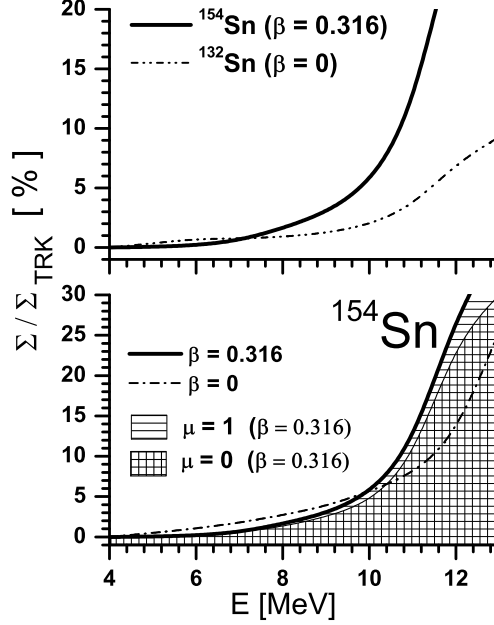
FIG. 6: The integrated photoabsorption cross section (16) in the percentage of the TRK sum rule Σ_{TRK}. The upper panel compares the cross sections for spherical ^{132}Sn and deformed ^{154}Sn. The bottom panel shows the cross sections in ^{154}Sn for the equilibrium deformation $\beta = 0.316$ and constrained spherical case $\beta = 0$. The contributions of $\mu = 0$ and $\mu = 1$ GDR branches for $\beta = 0.316$ are exhibited by areas with linear and check filling, respectively. The force SLy6 is used.

both branches become more comparable. Indeed, the $\mu = 0$ branch, being closer to the pygmy region, carries at the same time twice smaller strength than the $\mu = 1$ one. Hence the comparable effects of the branches at the remote energies. The deformation shifts the $\mu = 0$ and $\mu = 1$ branches in the opposite directions, thus leading to the deformation contributions of the opposite sign and comparable magnitude. These contributions compensate each other and drastically suppress the total deformation effect at the remote low energies. In principle, the rest effect can be of any sign, e.g. negative, as in our case. A weak negative deformation effect agrees with findings [8] and contradicts the assertion [22, 23] on its strong and positive magnitude.

IV.   CONCLUSIONS

The long chain of neutron-rich Sn isotopes with $132 \leq A \leq 166$ is investigated within the Skyrme RPA method by using SkT6, SkM*, SLy6, and SkI3 Skyrme forces. Both spherical and axially deformed shapes are considered. The smoothing effects beyond RPA are simulated by the double folding procedure which allows a direct computation of the strength function with the

energy dependent width.

All the Skyrme forces predict a region of prolate-soft isotopes $^{142-162}$Sn for which a strong anharmonicity in low-energy collective modes is expected. Though prolate shapes look surprising for the semi-magic Sn isotopes, they can be caused by the large neutron excess driving the system to deformations. The calculations also show that the pygmy E1 strength increases with the neutron number. Following our analysis, the nuclear deformation does not noticeably affect this trend and leads mainly to more spread and redistribution of the E1 strength. The effect of deformation on the cumulative E1 strength near the particle emission thresholds is shown to be small and negative (slight depletion of the strength). The result is explained by the compensation of the deformation contributions from $\mu = 0$ and $\mu = 1$ GDR branches. This finding may be of a significant interest for astrophysical applications.

The four Skyrme forces yield qualitatively similar results though their numerical predictions can vary for the total nuclear energy and fine structure of the pygmy mode. Our results are in a good agreement with the RMF study [8]

Acknowledgments

[1] N. Paar, D. Vretenar, E. Khan and G. Colo, *Rep. Prog. Phys.* **70**, 691 (2007).

[2] J. R. Stone and P.-G. Reinhard, *Prog. Part. Nucl. Phys.* **58**, 587 (2007).

[3] A. Wagner et al, *J. Phys.* **G35**, 014035 (2008).

[4] D. Savran et al, *Phys. Rev. Lett.* **97**, 172502 (2006).

[5] D. Savran et al, *Phys. Rev. Lett.* **100**, 232501 (2008).

[6] T. Anmann et al, *Nucl. Phys.* **A649**, 297c (1999).

[7] E. Tryggestad et al, *Nucl. Phys.* **A687**, 231c (2001).

[8] D. Peña Arteaga, E. Khan and P. Ring, *Phys. Rev.* **C79**, 034311 (2009).

[9] V.O. Nesterenko, J. Kvasil and P.-G. Reinhard, *Phys. Rev.* **C66**, 044307 (2002).

[10] V.O. Nesterenko, W. Kleinig, J. Kvasil, P. Vesely, P.-G. Reinhard, and D.S. Dolci, *Phys. Rev.* **C74**, 064306 (2006).

[11] V.O. Nesterenko, W. Kleinig, J. Kvasil, P. Vesely, and P.-G. Reinhard, *Int. J. Mod. Phys.* **E16**, 624 (2007).

[12] W. Kleinig, V.O. Nesterenko, J. Kvasil, P.-G. Reinhard, and P. Vesely, *Phys. Rev.* **C78**, 044313 (2008).

[13] P. Veselý, J. Kvasil, V.O. Nesterenko, W. Kleinig, P.-G. Reinhard, and V.Yu. Ponomarev, *Phys. Rev.* **C80**, 031302(R) (2009).

[14] V. O. Nesterenko, J. Kvasil, P. Veselý, W. Kleinig, P.-G. Reinhard and V. Yn. Ponomarev, *J. Phys. G* **37**, 064034 (2010).

[15] J. Kvasil, P. Vesely, V.O. Nesterenko W. Kleinig, P.-G. Reinhard, and S. Frauendorf, *Int. J. Mod. Phys.* **E18** 975 (2009).

[16] F. Tondeur, M. Brack, M. Farine, and J.M. Pearson, *Nucl. Phys.* **A420**, 297 (1984).

[17] J. Bartel et al, *Nucl. Phys.* **A386**, 79 (1982).

[18] E. Chabanat, P. Bonche, P. Haensel, J. Meyer, and R. Schaeffer, *Nucl. Phys.* **A627**, 710 (1997).

[19] P.-G. Reinhard and H. Flocard, *Nucl. Phys.* **A584**, 467 (1995).

[20] M. Bender, P.-H. Heenen and P.-G. Reinhard, *Rev. Mod. Phys.* **75**, 121 (2003).

[21] J.A. Maruhn, P.-G. Reinhard, P.D. Stevenson, J. Rikovska Stone, and M.R. Strayer, *Phys. Rev.* **C71**, 064328 (2005).

[22] F. Dönau, G. Rusev, R. Schwenner, A. R. Junghaus, K. D. Schilling and A. Wagner, *Phys. Rev.* **C76**, 014317 (2007).

[23] G. Rusev et al, *Phys. Rev.* **C79**, 061302 (2009).